

## Computational and Experimental Analyses Converge to Reveal a Coherent Yet Malleable Aptamer Structure That Controls Chemical Reactivity

Tianjiao Wang,<sup>†,‡</sup> Julie A. Hoy,<sup>‡</sup> Monica H. Lamm,<sup>§</sup> and Marit Nilsen-Hamilton\*,<sup>†,‡</sup>

Department of Biochemistry, Biophysics and Molecular Biology, Ames Laboratory, Macromolecular X-ray Crystallography Facility, Office of Biotechnology, and Department of Chemical and Biological Engineering, Iowa State University, Ames, Iowa 50011

Received April 9, 2009; E-mail: marit@iastate.edu

**Abstract:** As short nucleic acids, aptamers in solution are believed to be structurally flexible. Consistent with this view, most aptamers examined for this property have been shown to bind their target molecules by mechanisms that can be described as “induced fit”. But, it is not known to what extent this structural flexibility affects the integrity of the target–aptamer interaction. Using the malachite green aptamer (MGA) as a model system, we show that the MGA can protect its bound target, malachite green (MG), from oxidation over several days. Protection is reversed by an oligonucleotide complementary to the MGA binding pocket. Computational cavity analysis of the MGA-MG structure predicted that MG oxidation is protected because a molecule as small as an OH<sup>-</sup> is sterically excluded from the C1 position of the bound MG. These results suggest that, while the MGA-MG interface is sufficiently coherent to prevent OH<sup>-</sup> penetration, the bases involved in the interaction are sufficiently mobile that they can exchange out of the MG binding interface to hybridize with a complementary oligonucleotide. The computational predictions were confirmed experimentally using variants of the MGA with single base changes in the binding pocket. This work demonstrates the successful application of molecular dynamics simulations and cavity analysis in determining the effects of sequence variations on the structure of a small single-stranded nucleic acid. It also shows that a nucleic acid aptamer can control access to specific chemical groups on its target, which suggests that aptamers might be applied for selectively protecting small molecules from modification.

### Introduction

Aptamers are short, single-stranded nucleic acids that bind to their target molecules tightly with high specificities and that can be selected *in vitro* to recognize a large range of types and sizes of targets.<sup>1</sup> For protein structures, computational docking can often correctly identify potential molecular interactions by examining surface structural features. Also, certain protein binding pockets have been shown to exclude small molecules such as water from their bound targets.<sup>2–6</sup> For nucleic acid aptamers it has not been demonstrated that these more flexible polymers can adopt sufficiently rigid structures when complexed with their target molecules that they can exclude the entry of small molecules into the binding pocket. Short nucleic acids also sample more diverse structures in solution than do most proteins.<sup>7–9</sup> These structural changes upon target molecule

binding make modeling aptamer–target interactions more difficult than for most protein–target interactions.

The malachite green aptamer (MGA) binds one of two molecular targets, malachite green (MG) or tetramethylrosamine (TMR). Structural analyses of the MGA–target complexes show MG or TMR sitting in a binding pocket formed by the aptamer bases with less than 20% of the target exposed.<sup>10,11</sup> The aptamer pocket interacts differently with MG and TMR being modified in its structure by induced fit, which is a feature of the interaction of many aptamers with their targets.<sup>11–19</sup> Both aptamer and target molecule change in their structures during binding, with

- <sup>†</sup> Department of Biochemistry, Biophysics and Molecular Biology.  
<sup>‡</sup> Macromolecular X-ray Crystallography Facility, Office of Biotechnology.  
<sup>§</sup> Department of Chemical and Biological Engineering.  
<sup>‡</sup> Ames Laboratory.  
(1) Stoltenburg, R.; Reinemann, C.; Strehlitz, B. *Biomol. Eng.* **2007**, 24, 381–403.  
(2) Winkler, F. K.; D'Arcy, A.; Hunziker, W. *Nature* **1990**, 343, 771–774.  
(3) Kim, S. W.; Cha, S. S.; Cho, H. S.; Kim, J. S.; Ha, N. C.; Cho, M. J.; Joo, S.; Kim, K. K.; Choi, K. Y.; Oh, B. H. *Biochemistry* **1997**, 36, 14030–14036.  
(4) Sneeden, J. L.; Loeb, L. A. *J. Biol. Chem.* **2004**, 279, 40723–40728.

- (5) Wogulis, M.; Wheelock, C. E.; Kamita, S. G.; Hinton, A. C.; Whetstone, P. A.; Hammock, B. D.; Wilson, D. K. *Biochemistry* **2006**, 45, 4045–4057.  
(6) Schramm, A. M.; Mehra-Chaudhary, R.; Furdui, C. M.; Beamer, L. J. *Biochemistry* **2008**, 47, 9154–9162.  
(7) Getz, M.; Sun, X.; Casiano-Negroni, A.; Zhang, Q.; Al-Hashimi, H. M. *Biopolymers* **2007**, 86, 384–402.  
(8) Xia, T. *Curr. Opin. Chem. Biol.* **2008**, 12, 604–611.  
(9) Al-Hashimi, H. M.; Walter, N. G. *Curr. Opin. Struct. Biol.* **2008**, 18, 321–329.  
(10) Baugh, C.; Grate, D.; Wilson, C. *J. Mol. Biol.* **2000**, 301, 117–128.  
(11) Flinders, J.; DeFina, S. C.; Brackett, D. M.; Baugh, C.; Wilson, C.; Dieckmann, T. *ChemBioChem* **2004**, 5, 62–72.  
(12) Dieckmann, T.; Butcher, S. E.; Sassanfar, M.; Szostak, J. W.; Feigon, J. *J. Mol. Biol.* **1997**, 273, 467–478.  
(13) Patel, D. J.; Suri, A. K.; Jiang, F.; Jiang, L.; Fan, P.; Kumar, R. A.; Nonin, S. *J. Mol. Biol.* **1997**, 272, 645–664.  
(14) Williamson, J. R. *Nat. Struct. Biol.* **2000**, 7, 834–837.

the result that the flatter MG in the aptamer pocket has a much higher fluorescence output than unbound MG.<sup>20</sup>

The central carbon of MG is susceptible to attack by a base such as a hydroxide ion ( $\text{OH}^-$ ), which results in the formation of a colorless form (MG—OH). This reaction provides an opportunity to examine the extent to which the aptamer—target interaction is rigidly defined. If the aptamer—target complex samples a large range of structures, some of these structures might allow hydroxyl ions to slip into the core of the structure to oxidize the target molecule.

Computational analysis of protein—target interactions can aid experimental analysis when the results of amino acid residue exchanges can be tested in silico. Although molecular dynamics simulations have been used to examine the thermodynamic parameters associated with target molecule binding, the ability of computational analysis to accurately predict the structures of aptamers with altered sequences is not known. The availability of experimentally determined structures of the MGA-MG complex allowed us to test the ability of computational analysis (cavity analysis and molecular dynamics simulations) to accurately predict experimental results.

Malachite green is widely used as a dye in industry and as a fungicide in aquaculture. However, it is toxic and can promote cancer and embryonic defects.<sup>21–24</sup> The mechanism of MG toxicity is unknown but believed to involve its metabolism to more toxic forms. The investigation described here of the MG-MGA interaction shows for the first time that the reactivity of this chemical can be controlled by an aptamer, a polymer with the potential of in vivo function. This same concept might be extended to other reactive chemicals.

Here we analyzed the NMR structures of the MGA-MG complex by cavity analysis and molecular dynamics simulations and extended this analysis to simulations of aptamers with variations in sequence from the MGA. The computational analyses accurately predicted the results of experimental structural analyses of the MGA and its variants and their abilities to protect MG from oxidation. These studies show that, although it is a very flexible polymer, an aptamer can fold around its target molecule in a stable, tightly constrained structure that will not allow a molecule as small as a hydroxyl group to penetrate the complex over a period of days.

## Experimental Methods

**Chemicals and Oligonucleotides.** Malachite green oxalate (MG) was purchased from Sigma (St. Louis, MO). MG carbinol base (MG—OH) was prepared as follows: A 90 mL solution of 17 mg/mL MG in 0.5 M HEPES, pH 7.4, was left at 23 °C for 24 h. The

precipitated product was centrifuged at 1500 × g for 10 min. The pellet was collected and then dried at 74 °C for 6 h. All pHs reported here were measured at room temperature (~23 °C).

Oligonucleotides were synthesized by Integrated DNA Technologies, Inc. (Coralville, IA), or by the DNA Synthesis and Sequencing Facility at Iowa State University as listed: MGA,<sup>25</sup> GGAUC-CCGACUGGCGAGAGCCAGGUACGAAUGGAUCC; MGA (U25C), GGAUCCCCAAGCAAUGGAUC; MGA(A31C), GGA-UCCCCACUGGCCAGCUGGAUCC; MGA (G8C, G24C, G29C), GGAUCCCACUGGCCAGACUAACCAUGGAUCC; AS (antisense oligonucleotide that targets the region of MGA from G19 to C37), GATCCAGTTACCTGGC; and Shuffled AS (with the same bases but randomly shuffled with respect to the AS sequence), TCTCTAGAGTCTCTGCACG.

In addition to chemical synthesis, in vitro transcription by T7 RNA polymerase was also used to generate a 100 nt random sequence RNA pool: GGGAGACAAGAAUAAAAGCUCAA(N53)-UUCGACAGGAGGCUCACACAGGC.

**Mass Spectrometry.** Electrospray ionization of 1 mM MG in ddH<sub>2</sub>O was performed with a Finnigan TSQ700 triple quadrupole mass spectrometer (Finnigan MAT, San Jose, CA) fitted with a Finnigan ESI interface. The sample was introduced into the electrospray interface through an untreated fused-silica capillary with a 50 μm i.d. and 190 μm o.d. A mixture of 75 μg/mL horse skeletal muscle myoglobin and 12 μg/mL Met-Arg-Phe-Ala (MRFA) tetrapeptide in a 50:50 methanol/water solution was used for tuning and routine calibration of the instrument. The tuning mixture in a polypropylene vial was infused into the mass spectrometer at a rate of 3 μL/min on a Harvard Apparatus (model 22, South Natick, MA) syringe pump.

Electron impact ionization of MG—OH was performed on a TSQ700 triple quadrupole mass spectrometer (Finnigan MAT, San Jose, CA) fitted with a Finnigan EI/CI ion source. The sample was introduced into the mass spectrometer using the solids probe that was heated gradually from 100 to 400 °C. The instrument was used as a single quadrupole and scanned from 35 to 650 Da.

**NMR Spectrometry.** Solid state <sup>13</sup>C NMR spectra of MG and MG—OH were recorded at room temperature at 150 MHz by a Bruker AV-600 with CPTOSS as the pulse program.

<sup>1</sup>H NMR spectra of all samples were collected using a Bruker Avance 700 spectrometer equipped with a 5 mm HCN-Z gradient cryoprobe. All <sup>1</sup>H NMR spectra were acquired using a WATER-GATE pulse sequence with water flipback (Bruker sequence p3919fpgp) to minimize solvent saturation transfer. Spectra were averages of 512 transients. The spectral width was 18182 Hz (25 ppm). The samples were 100 μM MG, 50 μM MGA ± 100 μM MG, 50 μM MGA(U25C) ± 200 μM MG, 50 μM MGA(A31C) ± 100 μM MG, and 50 μM MGA(G8C-G24C-G29C) ± 500 μM MG. All samples were in 10 mM KH<sub>2</sub>PO<sub>4</sub>, 5 mM MgCl<sub>2</sub>, 10 mM KCl, pH 5.8, 5% D<sub>2</sub>O/95% H<sub>2</sub>O.

**Affinities of MGA Variants for MG.** Binding to the MGA variants causes the  $\lambda_{\max}$  of MG absorption to shift from 618 nm to between 629 and 632 nm depending on the variant.<sup>25</sup> The binding also enhances MG fluorescence.<sup>20</sup> On the basis of these properties, the affinities of the MGA variants were determined by UV-visible spectroscopy either using a Biowave S2100 diode array spectrophotometer (WPA, Cambridge, U.K.) or an ND-1000 spectrophotometer (NanoDrop, Wilmington, DE) or by a fluorescence spectrophotometer (Cary Eclipse, Variant, Palo Alto, CA). An antisense oligonucleotide that targets the region of MGA from G19 to C37 (AS) was used as a control for the effects of RNAs that interact with MG nonspecifically.

The UV-visible spectra were obtained of duplicated samples of MG and each MGA variant in buffers containing 100 mM Tris, 100 mM KCl, 5 mM MgCl<sub>2</sub>, pH 9.0. The concentrations of the MGA and variants were adjusted to ensure saturation of MG in

- (15) Merino, E. J.; Weeks, K. M. *J. Am. Chem. Soc.* **2003**, 125, 12370–12371.
- (16) Katilius, E.; Katiliene, Z.; Woodbury, N. W. *Anal. Chem.* **2006**, 78, 6484–6489.
- (17) Lee, J. H.; Jucker, F.; Pardi, A. *FEBS Lett.* **2008**, 582, 1835–1839.
- (18) Lin, P. H.; Yen, S. L.; Lin, M. S.; Chang, Y.; Louis, S. R.; Higuchi, A.; Chen, W. Y. *J. Phys. Chem. B* **2008**, 112, 6665–73.
- (19) Hermann, T.; Patel, D. J. *Science* **2000**, 287, 820–825.
- (20) Babendure, J. R.; Adams, S. R.; Tsien, R. Y. *J. Am. Chem. Soc.* **2003**, 125, 14716–14717.
- (21) Kraus, G. A.; Jeon, I.; Nilsen-Hamilton, M.; Awad, A. M.; Banerjee, J.; Parvin, B. *Molecules* **2008**, 13, 986–994.
- (22) Mittelstaedt, R. A.; Mei, N.; Webb, P. J.; Shaddock, J. G.; Dobrovolsky, V. N.; McGarry, L. J.; Morris, S. M.; Chen, T.; Beland, F. A.; Greenlees, K. J.; Hefflich, R. H. *Mutat. Res.* **2004**, 561, 127–138.
- (23) Culp, S. J.; Mellick, P. W.; Trotter, R. W.; Greenlees, K. J.; Kodell, R. L.; Beland, F. A. *Food Chem. Toxicol.* **2006**, 44, 1204–1212.
- (24) Jang, G. H.; Park, I. S.; Lee, S. H.; Huh, T. L.; Lee, Y. M. *Biochem. Biophys. Res. Commun.* **2009**, 382, 486–491.

- (25) Grate, D.; Wilson, C. *Proc. Natl. Acad. Sci. U.S.A.* **1999**, 96, 6131–6136.

each case with at least six different concentrations of the RNA. The  $\lambda_{\max}$  for each scan was recorded and plotted against the concentration of the appropriate MGA variant or control RNA (AS). The plots were fitted to  $\lambda = \lambda_0 + \Delta\lambda[M]/(K_d + [M])$  using a nonlinear regression function in the Costat program (CoHort Software, Monterey, CA), where  $\lambda$  is the maximal absorption wavelength of MG in the presence of different concentrations of the RNA,  $\lambda_0$  is the maximal absorption wavelength of free MG,  $\Delta\lambda$  is the difference of maximal absorption wavelengths between free MG and MG saturated with each RNA,  $K_d$  is the dissociation constant, and  $[M]$  is the concentration of the RNA.

To obtain  $K_d$ -values of the interaction of MG with MGA or its variants, the fluorescence emission spectra for MG were determined in 100 mM Tris, 100 mM KCl, 5 mM MgCl<sub>2</sub>, and pH 9.0 alone and in the presence of each of 11 different concentrations of each RNA. The samples were excited at 630 nm and the emission spectra were recorded from 640–700 nm with 650 nm as the maximal emission wavelength. The data were fit to  $F_{650}/F_{\max} = [M]/(K_d + [M])$  using the Costat program where  $F_{650}$  is the fluorescence intensity at 650 nm of samples,  $F_{\max}$  is the  $F_{650}$  when MG is completely saturated,  $[M]$  is the concentrations of the MGA variants, and  $K_d$  is the dissociation constant for MG and the MGA or its variants.

**Kinetics of MG–OH Formation.** The UV–visible spectra of MG, with or without each RNA, in buffers containing either 10 mM HEPES, 100 mM KCl, 5 mM MgCl<sub>2</sub>, pH 7.2–7.4 (Figure 1) or 100 mM Tris, 100 mM KCl, 5 mM MgCl<sub>2</sub>, pH 9.0 (Figure 3), were determined by using either a Biowave S2100 diode array spectrophotometer (WPA, Cambridge, U.K.) or a ND-1000 spectrophotometer (NanoDrop, Wilmington, DE). At least three independent experiments were done of each described condition. The rates of production of MG–OH were monitored for up to 46 h by recording  $A(\lambda_{\max})$ . The  $\lambda_{\max}$  ranged from 618 to 632 nm depending on the concentration and the MGA variants. Then  $A(\lambda_{\max})$  was plotted against time and fitted by a nonlinear regression function in Costat to the equations  $A = A_0 \exp(-kt)$  for MG alone at pH > 8 and  $A = A_0/(1 + ktC_0)$  for all others, where  $A_0$  is the  $A(\lambda_{\max})$  at  $t = 0$ ,  $A$  is the  $A(\lambda_{\max})$  at each time point,  $k$  is the reaction rate,  $t$  is the time, and  $C_0$  is the initial concentration of MG. The half-life of MG–OH formation was calculated with the best fit as  $t_{1/2} = 0.693/k$  (MG alone at pH > 8) and  $t_{1/2} = 1/kC_0$  (MG alone at pH < 8 and in the presence of MGA and its variants). The statistical analysis of the means of the  $t_{1/2}$  of MG from Supporting Information Table S1 were done in R, first by F-test and then by Tukey multiple comparisons of mean values (Supporting Information Table S2).<sup>26,27</sup>

**Molecular Dynamics (MD) Simulations of MGA-MG Variants.** MD simulation of the MGA-MG variant complexes were carried out with NAMD2.6 that was developed by the Theoretical and Computational Biophysics Group in the Beckman Institute for Advanced Science and Technology at the University of Illinois, Urbana-Champaign (<http://www.ks.uiuc.edu/Research/namd/>, accessed May 24, 2009).<sup>28</sup> The setup for simulation and analysis of the simulation results were done with VMD1.8.6 (<http://www.ks.uiuc.edu/Research/vmd/>, accessed May 24, 2009).<sup>29</sup> The CHARMM topology file (top\_all27\_prot\_na.rtf.) and the parameter file (par\_all27\_prot\_na.prm)<sup>30</sup> were modified to include MG for setting up and running the simulation. For

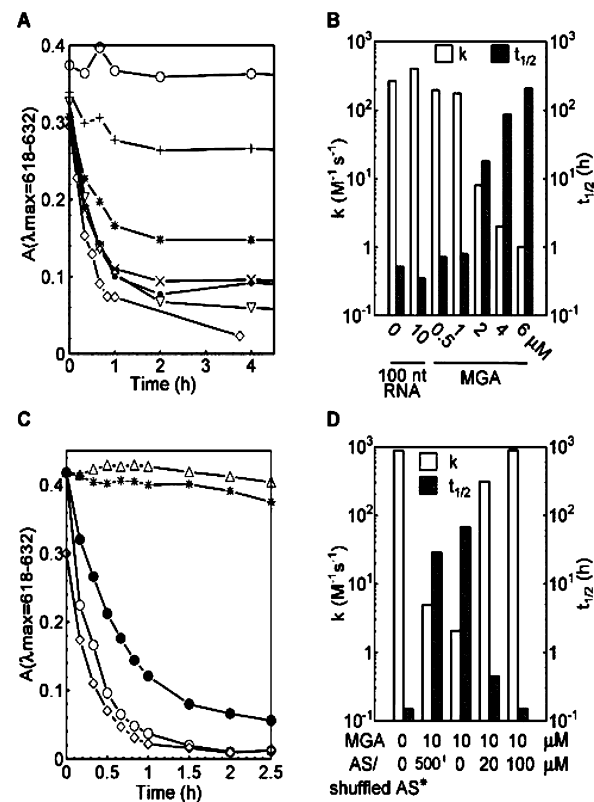


**Figure 1.** Malachite green aptamer protects MG from oxidation. A, B: The kinetics of MG oxidation in the presence of MGA or control RNA. Two micromolar MG was incubated in the absence ( $\nabla$ ) or presence ( $\diamond$ ) of 10  $\mu$ M 100 nt random RNA pool or in the presence of various concentrations of the MGA: 0.5  $\mu$ M ( $\bullet$ ), 1  $\mu$ M ( $\times$ ), 2  $\mu$ M (\*), 4  $\mu$ M (+), 6  $\mu$ M ( $\circ$ ) MGA. C, D: The kinetics of MG oxidation in the presence of the MGA and varying concentrations of AS. Two  $\mu$ M MG was incubated for 2 min alone ( $\diamond$ ) or with 10  $\mu$ M MGA ( $\triangle$ ). To this mixture was then added 50  $\mu$ M shuffled AS (\*) or AS at concentrations of 20  $\mu$ M ( $\bullet$ ) or 100  $\mu$ M ( $\circ$ ). A, C: The changes in MG color were tracked as a function of time. B, D: The constants  $k$  and  $t_{1/2}$  were determined from the plots in A and C. The figure shows the results of one of three independent experiments, each of which gave consistent results.

MG, the topology and parameter files (see Supporting Information) were generated manually according to previously reported quantum-chemical calculations.<sup>31</sup>

The procedure is described briefly as follows. The MGA-MG complex (PDB ID: 1Q8N, model 5)<sup>11</sup> and the MGA(A31C)-MG and MGA(U25C)-MG derived from variations in the sequence of the MGA by using the Coot package<sup>32</sup> were solvated in a water box (76 Å × 52 Å × 50 Å) containing 9261 TIP3P H<sub>2</sub>O. Ions (19 Mg<sup>2+</sup> and 1 Cl<sup>-</sup>) were added to the solvated systems using the Meadionize plugin 1.1 developed by Ilya Balabin, Duke University (<http://www.chem.duke.edu/~ilya/Software/Meadionize/docs/meadionize.html>, accessed May 24, 2009). The solvated and ionized systems were then run on NAMD with the CHARMM force field. For the simulation parameters, the electrostatic and van der Waals interaction distance cutoff was set to 12 Å. The full-system periodic electrostatics was calculated with a particle mesh Ewald summation of ~1 Å grid space. The time step was set to 2 fs. After 5000 steps of minimization, the unconstrained simulation was run under a periodic boundary condition at a constant temperature (298 K) and pressure (1.01325 bar) for 5.4 ns for MGA-MG, 5.6 ns for MGA-MG(A31C), and 7.9 ns for MGA-MG(U25C).

- (26) *Multiple comparisons, selection, and applications in biometry: a festschrift in honor of Charles W. Dunnett*; Hoppe, F. M., Ed.; Dekker: New York, NY, 1993.
- (27) R\_Development\_Core\_Team; R Foundation for Statistical Computing: Vienna, Austria, 2009.
- (28) Phillips, J. C.; Braun, R.; Wang, W.; Gumbart, J.; Tajkhorshid, E.; Villa, E.; Chipot, C.; Skeel, R. D.; Kale, L.; Schulten, K. *J. Comput. Chem.* **2005**, *26*, 1781–1802.
- (29) Humphrey, W.; Dalke, A.; Schulten, K. *J. Mol. Graph.* **1996**, *14*, 33–38.
- (30) MacKerell, A. D., Jr.; Banavali, N.; Foloppe, N. *Biopolymers* **2000**, *56*, 257–265.

- (31) Nguyen, D. H.; DeFina, S. C.; Fink, W. H.; Dieckmann, T. *J. Am. Chem. Soc.* **2002**, *124*, 15081–15084.
- (32) Emsley, P.; Cowtan, K. *Acta Crystallogr., Sect. D* **2004**, *60*, 2126–2132.

**Cavity Analysis of Free MG and the MGA-MG Variants.** Analysis of the 25 NMR structures of the MGA-MG complex (1Q8N.pdb) by LSQMAN<sup>33</sup> indicates that the central chain is model 5 and the average rmsd between chains = 0.709 Å (using C4\* P C1\* C2\* C3\* O2\* O3\* O4\* atoms to align chains). Model 15 has the highest deviation from model 5 with the rmsd between chains = 0.870 Å; thus both models 5 and 15 were analyzed for cavities. Because no important differences were found between these two models, only the results for model 5 are reported. Analysis of the simulated structures of the MGA-MG variants was done by VMD. Simulated structures with high RMSDs from the 1Q8N.pdb model 5 starting structure (especially for residues 8, 28, and 39) were chosen for cavity analysis. The reason for these choices was to determine if the variant molecules sampled structures that were different enough from the original MGA structure to result in the creation of a channel for OH<sup>-</sup> entry. Cavity analysis of the MGA variants' binding pockets and free MG were performed using SURFNET.<sup>34</sup> A radius of 1.32 Å was chosen as the smallest possible radius for an hydroxide ion<sup>35</sup> while the maximum radius was set to 1.9 Å. The figure was created with SPDBV,<sup>36</sup> PyMol (Delano Scientific LLC, <http://www.pymol.org>, accessed May 24, 2009) and POV-Ray (Persistence of Vision Raytracer Pty. Ltd.).

**Structural Probing of the MGA Variants.** RNase I footprinting was used to study the structural alterations of the binding pocket of the MGA due to sequence variations (A31C, U25C, and G8C-G24C-G29C). RNase I can cleave RNAs in single-stranded but not in double-stranded regions. The MGA variants, including MGA, MGA(A31C), MGA(U25C), and MGA(G8C-G24C-G29C), were first labeled with  $\gamma$ -<sup>32</sup>P-ATP (MP Biomedicals, Solon, OH) by T4 polynucleotide kinase (Promega, Madison, WI) at their 5'-ends. Twenty microliters of labeling reaction mixtures containing 5 μM RNA, 1.5 μCi/μL  $\gamma$ -<sup>32</sup>P-ATP, 1 U/μL T4 polynucleotide kinase, 70 mM Tris-HCl (pH 7.6), 10 mM MgCl<sub>2</sub>, and 5 mM DTT were incubated for 1.5 h at 37 °C. The labeled MGA variants were purified by electrophoresis through 10% polyacrylamide gels in the presence of 7 M urea and then incubated with RNase I in the presence or absence of MG to probe the RNA structure. Reaction mixtures of 10 μL containing 0.125 μM <sup>32</sup>P-labeled RNA, 0.5 × 10<sup>-4</sup> U/μL RNase I, 100 mM KCl, 5 mM MgCl<sub>2</sub>, 10 mM HEPES, pH 7.4, were incubated at 23 °C for 10 min in the absence or presence of MG. Partial alkaline hydrolysis of the labeled RNAs was done in 50 μM Na<sub>2</sub>CO<sub>3</sub>, pH 9.0 at 95 °C for 5 min. RNase T1 digestion of the labeled RNAs was carried out in 10 μL reaction mixture containing 0.5–1 U/μL RNase T1, 5 M urea, 350 mM sodium citrate, 0.7 mM EDTA, pH 5.0, at 50 °C for 4 min. The RNA hydrolysis and cleavage reactions were stopped by bringing the reaction mixtures to 47.5% formamide, 0.05% bromophenol blue, and 0.05% xylene cyanol FF. The samples were resolved by electrophoresis through 10% polyacrylamide gels in the presence of 7 M urea. The radioactivity was recorded from the dried gels using a phosphor screen and imaged with a Typhoon 8600 Variable Model Imager (GE Healthcare, Piscataway, NJ).

## Results

**Oxidation of MG.** MG loses color by a mechanism that is pH-dependent, and the data for MG at pHs above 8 fit best to a first order kinetic equation, whereas the data for MG at pHs less than 8 fit best to a second order equation. The results are consistent with the bleaching kinetics at above pH 8 being pseudo-first order (Supporting Information Figure S1). The chemical form of the bleached MG was characterized by mass spectrometry and NMR spectroscopy. The mass spectrum of

MG had an expected peak at *m/z* 329, and the MG-OH spectrum contained an additional *m/z* 346 peak as expected of hydroxylated MG (Supporting Information Figure S2A). In the NMR spectra of MG and MG-OH, the C1 peak was shifted from the 175.91 ppm in MG to 82.59 ppm in MG-OH. The C11 of MG at 165.115 ppm was shifted to 149.08 ppm in MG-OH, and the double peaks of N(CH<sub>3</sub>)<sub>2</sub> and +N(CH<sub>3</sub>)<sub>2</sub> (40.91 ppm and 39.95 ppm) in MG became a single peak of N(CH<sub>3</sub>)<sub>2</sub> (40.39 ppm) in MG-OH (Supporting Information Figure S2B). These results are consistent with the conclusion that MG-OH is hydroxylated at C1 and that the bleached MG is in the form of a carbinol base (Supporting Information Figure S2C).

**MGA Binding Pocket Protects MG from Oxidation.** Because the MGA binding pocket is formed by bases that lie above and below MG, it seemed possible that the MGA might protect MG from oxidation by sterically hindering the entrance of OH<sup>-</sup> into the binding pocket. We tested this hypothesis by incubating MG with various concentrations of the MGA and found that the MGA inhibited MG oxidation with a dependence on MGA concentration (Figure 1A,B). At 6 μM MGA, a concentration that is about 6 times the *K*<sub>d</sub> for the MGA-MG interaction, the rate of MG oxidation was almost zero. By contrast, 10 μM 100 nt random sequence RNA pool had no effect on the rate of MG to MG-OH oxidation (Figure 1A,B).

If the MGA protects the MG in its binding pocket from hydroxyl attack, then a distortion of the binding pocket should result in loss of its effect on MG oxidation. This result was observed in experiments in which the reaction mixture included an oligonucleotide (AS) with a sequence complementary to bases 19 to 37 in the MGA sequence that constitutes one-half of the MG-binding pocket. Addition of AS (but not its shuffled sequence version) to a mixture of MGA and MG reversed the protection by MGA of MG oxidation with ~30% reversal at 2AS/MGA and almost complete reversal at 10AS/MGA (Figure 1C,D).

**Cavity Analysis of the MGA-MG Complex Shows No Gap for OH<sup>-</sup> Entry.** Our results suggested that the ability of the MGA to inhibit oxidation of MG is because the MGA-MG complex sterically hinders OH<sup>-</sup> access to the C1 of the MG located in the binding pocket. As a result of the very small size of OH<sup>-</sup>, this condition requires a very snug fit of MG in the binding pocket of the MGA. Cavity analysis was used to test the hypothesis. With the route of OH<sup>-</sup> attack on MG being limited by the equatorial phenyl rings, anion attack can only proceed by polar routes (Figure 2B,C). However, cavity analysis showed that, while sitting in the MGA binding pocket, MG was protected from polar attack by G8-C28 and C7-G29-G24-A31, which does not allow a gap of the minimum size of an OH<sup>-</sup> group to reach C1 from the solvent surface of the MGA (Figure 2D).

**Changes in the MGA Binding Pocket Sequence Compromise the Ability of the MGA To Protect MG Oxidation.** To test the hypothesis that steric hindrance in the MGA binding pocket prevents hydroxyl attack, variants of the MGA with base changes around the binding pocket were made including MGA(A31C), MGA(U25C), and MGA(G8C-G24C-G29C). These changes were chosen based on their locations in the binding pocket (Figure 2A) and the results of cavity analysis.

The *K*<sub>d</sub> of each MGA variant for MG was measured (Table 1), and a concentration of each MGA variant equivalent to 10–15 times of its *K*<sub>d</sub> was chosen at which MG would be saturated by the RNA. With these concentrations the rate of MG oxidation was negligible in the presence of the MGA,

(33) Kleywegt, G. J. *Acta Crystallogr., Sect. D* **1996**, *52*, 842–857.

(34) Laskowski, R. A. *J. Mol. Graph.* **1995**, *13*, 323–330.

(35) Fox, M.; McIntyre, R.; Hayon, E. *Faraday Discuss. Chem. Soc.* **1977**, *64*, 167–172.

(36) Guex, N.; Peitsch, M. C. *Electrophoresis* **1997**, *18*, 2714–2723.

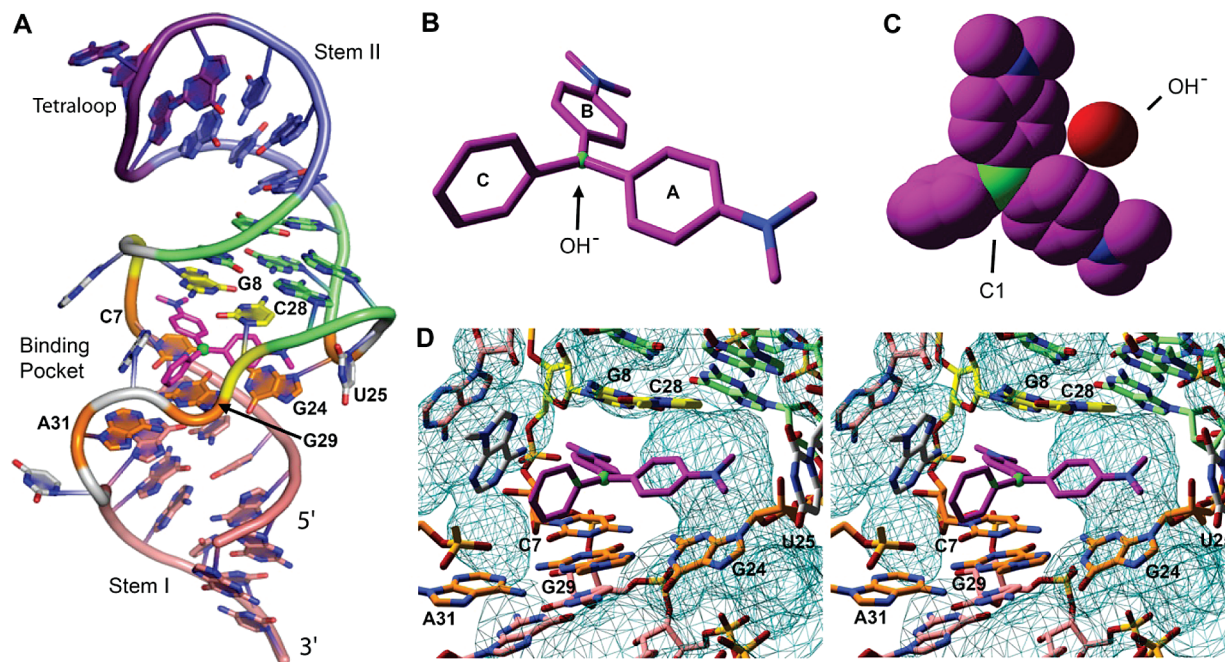


**Figure 2.** Cavity analysis by Surfnet of MG alone and in the MGA binding pocket. (A) MG (magenta) is flanked in the binding pocket of MGA (1q8n.pdb, model 5) by C7, G24, G29, and A31 (orange) on one side and G8 and C28 (yellow) on the other. Stem I (red), the base triples (green), stem II (blue), and the tetraloop (purple) are also shown. (B) MG contains three aromatic rings around the central carbon (green). Hydroxide molecules can attack from above or below the plane, but (C) the rings block approach within the plane of the ring. (D) Stereoview of the MG binding pocket of MGA, colored as above, with cyan mesh indicating the area accessible to an hydroxide of minimum radius. The space above and below the plane of MG is blocked by the bases of the binding pocket and is therefore not accessible, as indicated by the lack of mesh. The foreground of the image has been slabbed away to assist in viewing the interior of the binding pocket.

**Table 1.** Affinities and  $\lambda_{\max}$  of the Interaction of MG with the MGA and Its Variants<sup>a</sup>

RNA	MG	$K_d$ ( $\mu$ M)	$\lambda_{\max}$ (nm)	$t_{1/2}$ of MG oxidation (h)
MGA	0.1–15 $\mu$ M	0.2 $\mu$ M	1.03 ± 0.53	632
MGA(A31C)	0.1–15 $\mu$ M	0.2 $\mu$ M	1.93 ± 0.97	24
MGA(U25C)	1–400 $\mu$ M	0.4, 2 $\mu$ M	13.8 ± 3.40	24
MGA(G8C-G24C-G29C)	0.025–1.7 mM	20 $\mu$ M	274 ± 65	5.5
AS	0.025–1.2 mM	20 $\mu$ M	172 ± 13	ND
none		2, 20 $\mu$ M	618	0.82

<sup>a</sup> The MGA, MGA variants, and AS were tested for their abilities to bind MG. The  $K_d$  values were determined using the concentrations of MG and RNAs shown in the table. The  $t_{1/2}$  of MG oxidation was measured in the presence of concentrations equivalent to  $10–15 \times K_d$  of the MGA variants. The data for  $t_{1/2}$  are derived from the fitting curves of the averages of four to nine independent experiments (Figure 3). The equations that gave the best fit were used in each case. For MG alone (none) the equation was first order, and for all others the best fitting equation was second order. The average residuals for the fits of each plot were <7%. In each independent experiment the relative order of  $t_{1/2}$  values [MGA ≫ MGA(A31C), MGA(U25C) > MGA(G8C-G24C-G29C), none] was the same as for the average values shown here (Supporting Information Figure S3). The  $p$  values for the Tukey comparisons between the treatments were <10<sup>-8</sup>, except 0.327 for the comparison between MGA(A31C) and MGA(U25C) and 0.175 for the comparison between MGA(G8C-G24C-G29C) and none (Supporting Information Tables S1 and S2). ND, not determined. UD, undetectable.

intermediate for the MGA(A31C) and MGA(U25C) and large for the MGA(G8C-G24C-G29C) (Figure 3 and Supporting Information Figure S3 and Table 1 and Supporting Information Tables S1 and S2).

**Structural Probing Shows Structurally Altered MG Binding Pockets in the MGA Variants.** To determine whether there are structural changes in the binding pockets, RNase I footprinting was performed of the MGA variants in the presence of various concentrations of MG. The data showed that MG binding to the MGA protected the binding pocket and destabilized the tetraloop (Figure 4A). The MGA(A31C) showed a similar cleavage pattern to the MGA except there was increased cleavage of U32 and C31 (Figure 4B). A similar cleavage pattern was observed of the MGA(U25C), as for the MGA (Figure 4C). By contrast, the footprinting pattern of MGA(G8C-G24C-G29C) showed all regions protected except C29 in three of four experiments (Figure 4D).

**<sup>1</sup>H NMR Spectra Are Consistent with Proper Folding of the MGA Variants and Binding of MG to Each MGA Variant.** To determine whether the MGA variants still folded properly and bound MG, <sup>1</sup>H NMR spectra were acquired for the MGA variants in the presence and absence of MG. The spectrum of MG alone was also acquired as a control, which showed sharp peaks in the 6.8–6.9, 7.25–7.35, 7.45–7.50, and 7.60–7.65 ppm regions (Figure 5). These peaks were similarly broadened in the presence of the MGA and each MGA variant, indicating a similar binding mode of MG to the MGA variants as to MGA.

The number of peaks from the MGA variants in the 10–15 ppm region, which references the base-pairings in the MGA structure, was 9–10 for the MGA and all its variants in the absence of MG. In the presence of MG, there were 13–14 peaks for MGA, MGA(A31C), and MGA(U25C) and 7 for MGA(G8C-G24C-G29C). These results are consistent with the conclusion

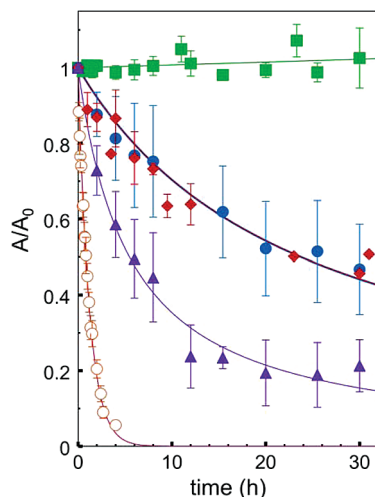


**Figure 3.** Variations around the MGA binding pocket compromise its ability to protect MG. MG oxidation in the presence of the MGA variants at concentrations equivalent to 10–15 times  $K_d$  was measured spectrophotometrically. The concentrations of interacting components were 3 or 30  $\mu\text{M}$  MG (orange ○), 3  $\mu\text{M}$  MG, 10  $\mu\text{M}$  MGA (green ■), 3  $\mu\text{M}$  MG, 20–30  $\mu\text{M}$  MGA(A31C) (blue ●), 30  $\mu\text{M}$  MG, 140–200  $\mu\text{M}$  MGA(U25C) (red ♦), 30  $\mu\text{M}$  MG, 3 mM MGA(G8C, G24C, G29C) (purple ▲). The figure shows the averages of the results of four to nine independent experiments with standard deviations for the MGA and each MGA variant. The fitting curves for MGA(A31C) and MGA(U25C) are identical. All experiments gave consistent results of the  $t_{1/2}$ s following the relationship of MGA ≫ MGA(A31C), MGA(U25C) > MGA(G8C-G24C-G29C), No RNA.

that, except for MGA(G8C-G24C-G29C), the MGA variants fold properly into structures similar to MGA that can bind MG in a defined binding pocket.

In the presence of MG the NMR spectra of the MGA and MGA variants differed, especially in the 6.5 to 9.0 ppm range where the proton exchange rates are not affected by pH, salt, and other buffer conditions. We interpret these results to show that MGA and its variants fold into similar, but nonidentical, structures, each of which binds MG.

**Cavity Analysis of Simulated MGA-MG Variants Shows Routes for OH<sup>-</sup> Access to the C1 of MG in the Binding Pockets of the MGA Variants.** To determine if MD simulation of the MGA variants could predict the observed accessibility of the bound MG to oxidation, we performed MD simulation followed by cavity analysis of the variants. The MD simulations reached equilibrium after 0.5–1.5 ns as judged by constant temperature (298 K), minimal energy, and stable root-mean-square deviation (rmsd; data not shown). The coordinates of the MGA-MG variants were allowed to further evolve for 4.2–6.4 ns. The equilibrated structures with high rmsd (especially the positions of residues 8 and 28 relative to MG) from the starting NMR structures were chosen for cavity analysis.

Cavity analysis of the simulated MGA-MG showed no gap for OH<sup>-</sup> access to C1 of MG inside the MGA binding pocket as already found for the NMR structure of MGA-MG (Figure 2). By contrast, the simulated MGA(A31C)-MG and MGA(U25C)-MG complexes showed routes for OH<sup>-</sup> access to C1 of MG in the pocket (Figure 6).

In the NMR and simulated MGA-MG structures, A31 and G24 interact as a quadruple with base-paired C7 and G29. While C7, G29, and G24 interact with the plane of MG, base A31 maintains the orientation of the other three members of the quadruple but does not stack with MG (Figure 6A). This arrangement changes in the simulated MGA(A31C)-MG struc-

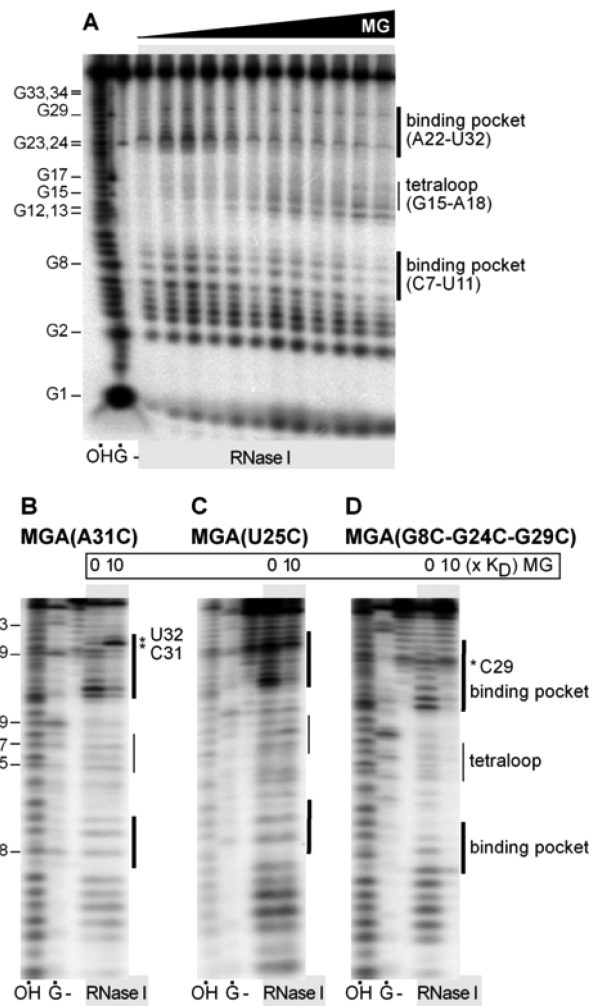


**Figure 4.** Footprinting analysis of the binding pockets of the MGA variants. RNase I footprinting of (A) the MGA with and without increasing MG concentrations (0.05 to 4  $\mu\text{M}$ ), (B) the MGA(A31C) with and without 20  $\mu\text{M}$  MG that was equivalent to 10 times  $K_d$ , (C) the MGA(U25C) with and without 140  $\mu\text{M}$  MG that was equivalent to 10 times  $K_d$ , and (D) the MGA(G8C-G24C-G29C) with and without 3 mM MG that was equivalent to 10 times  $K_d$ . Each experiment was repeated at least twice with similar results.

ture, in which the smaller size of C compared to A allows a shift of C7 and G29 toward C31, exposing the two nitrogenated phenols of MG. The G24 of MGA(A31C)-MG is not part of the quadruple and instead is in a position perpendicular to the two nitrogenated phenols of MG (Figure 6B). This assists in holding MG in the pocket but allows solvent entry on both sides of the plane of MG. On the C7/G29 side, C1 is not quite exposed enough for OH<sup>-</sup> attack in MGA(A31C)-MG. However, there is a cavity in this variant in the pocket on the G8/C28 side.

In the MGA pocket, G8 and C28 stack directly over the nitrogenated phenols of MG preventing access to C1 of MG (Figure 6A). However, in the simulated MGA(A31C)-MG structures in which a gap is found by cavity analysis, the shift in position between MG and the quadruple is associated with a shift of MG relative to G8-C28 where stacking of G8 and C28 occurs with one nitrogenated phenol and the un-nitrogenated phenol, leaving the second nitrogenated phenol and C1 exposed to OH<sup>-</sup> attack on the G8-C28 side (Figure 6B).

In the simulated MGA(U25C)-MG structure in which a gap was found, the G29 on the quadruple side of MGA(U25C) is

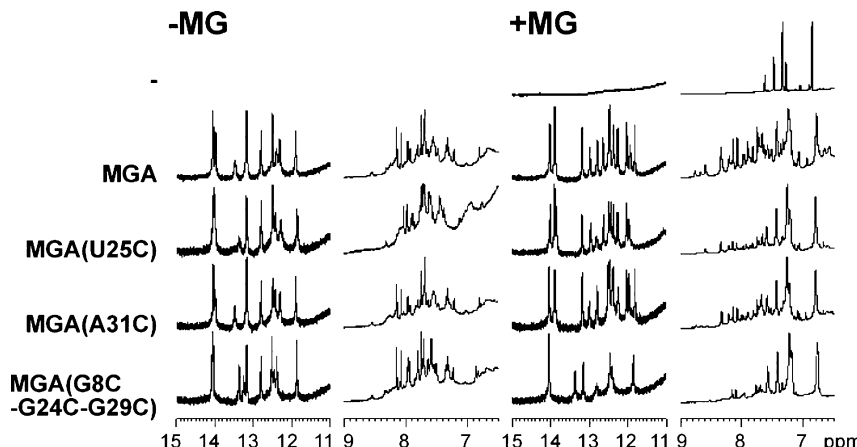


**Figure 5.**  $^1\text{H}$  NMR spectra showed proper folding of the MGA variants and evidence of MG binding. The  $^1\text{H}$  NMR spectra includes two regions: 11–15 ppm and 6.5–9.0 ppm.

most involved with MG stacking, although C7, G29, and A31 maintain their quadruple orientations to each other and C1 remains protected on this side. G24 is not a part of the quadruple in MGA(U25C)-MG; therefore, the quadruple has become a triple in this MGA variant. On the G8/C28 side, U25 lines a side of the pocket, perpendicular to MG, without forming H-bonds in MGA-MG (Figure 6A). However, because of the charge difference between U and C, the C25 in the simulated MGA(U25C)-MG is shifted to the G8/C28 side of MG, angled by  $\sim 45^\circ$  to MG, enabling hydrogen bonding to A27 and C28. This interaction again shifts the G8/C28 stacking with the MG to one nitrogenated phenol and the unmodified phenol, leaving the other nitrogenated phenol and C1 exposed to  $\text{OH}^-$  attack on this side (Figure 6C). G24 shifts in position with C25, decreasing its ability to block MG from leaving the pocket. This latter observation is consistent with the experimental observation of a lower affinity of MGA(U25C) for MG.

Thus, MD simulation followed by cavity analysis of the MG variants A31C and U25C resulted in predictions, confirmed by experimental results, that both variants could only partially protect MG from oxidation and that the A31C variant should have a higher affinity for MG than the U25C variant.

## Discussion

MG is held tightly in the pocket of the MGA that is created by a bulge between two short stems resulting in a structurally modified MG.<sup>31</sup> Our results show that this interaction is so snug that it prevents access of a molecule as small as a hydroxyl ion to the central carbon of MG. During the period that MG sits in the MGA pocket the MD simulation shows that the ligand and aptamer move in concert with the result that, despite movement of the aptamer, the ligand appears continuously protected. When the ligand is released by the aptamer it is expected to be susceptible to oxidation. However, there was no evidence of MG oxidation over a several day period when in the presence of saturating concentrations of the MGA. The explanation is likely the kinetics. The MGA-MG interaction is characterized by  $k_{\text{on}} = 2.32 \pm 0.76 \times 10^6 \text{ M}^{-1} \text{ s}^{-1}$ ,  $k_{\text{off}} = 0.39 \pm 0.13 \text{ s}^{-1}$ , and dissociation half-life =  $1.8 \pm 0.83 \text{ s}$  (Wang, unpublished data). By contrast, the MG oxidation reaction half-life is much longer at  $0.70 \pm 0.07 \text{ h}$ . Thus, although the MGA-MG interaction involves a dynamic exchange of bound and free MG, the kinetics of the MGA-MG interaction is too fast to allow measurable MG modification of the free MG when in the presence of saturating concentrations of the MGA.

We characterized the MG oxidation by UV-visible spectrophotometry, mass spectrometry, and NMR spectrometry. The results of these studies suggest that the most likely form of MG-OH contains a carbinol group at position C1. MG oxidation is also pH-dependent and second order at pH's below 8. Thus, it appears that the C1 of MG is attacked by an  $\text{OH}^-$  to form MG-OH. This reaction product was also predicted in a study of MG oxidation in alkaline solution.<sup>37</sup>

The MGA inhibits MG oxidation in a concentration-dependent manner with a stoichiometry that suggests steric hindrance rather than a catalytic mechanism. The specificity of the effect of the MGA on MG was demonstrated by the observation that a high concentration of a random sequence RNA pool has little effect on the rate of MG oxidation. The ability of an oligonucleotide (AS), complementary to the binding pocket of the MGA, to reverse the effect of the MGA on MG oxidation showed that the MGA must bind MG to prevent oxidation. Similar reversibility has been shown in other systems in which the activities of aptamers are regulated.<sup>38,39</sup>

Several mechanisms were considered for how the MGA could protect MG from  $\text{OH}^-$  attack. First, the MGA could alter the charge on C1 to make it less susceptible to  $\text{OH}^-$  attack. The MGA has been shown to change the charge distribution across MG, but physical chemical calculations showed that C1 is more positively charged in the MGA-MG complex compared to in solution.<sup>31</sup> A more positively charged MG would be more susceptible to  $\text{OH}^-$  attack rather than less as we have observed. By this analysis, we excluded charge distribution as the mechanism by which the MGA prevents MG oxidation. Second, the aptamer could inhibit MG oxidation by kinetic hindrance. However, there is no relation between the kinetic parameters of the MGA variants and the MG hydroxylation rate. Whereas MGA and MGA(31C) have the same affinities for MG but different effects on MG oxidation, MGA(31C) and MGA(U25C) have different affinities for MG but the same effect on MG oxidation.

To test the hypothesis, that the MGA might protect MG from oxidation by steric hindrance, we carried out a computational structural analysis of the MGA-MG complex<sup>11</sup> and free MG. The results of these studies showed that the rings A, B, and C

(37) Chen, D.; Laidler, K. *Can. J. Chem.* **1959**, *37*, 599–611.

(38) Cong, X.; Nilsen-Hamilton, M. *Biochemistry* **2005**, *44*, 7945–7954.

(39) Rusconi, C. P.; Scardino, E.; Layzer, J.; Pitoc, G. A.; Ortell, T. L.; Monroe, D.; Sullenger, B. A. *Nature* **2002**, *419*, 90–94.

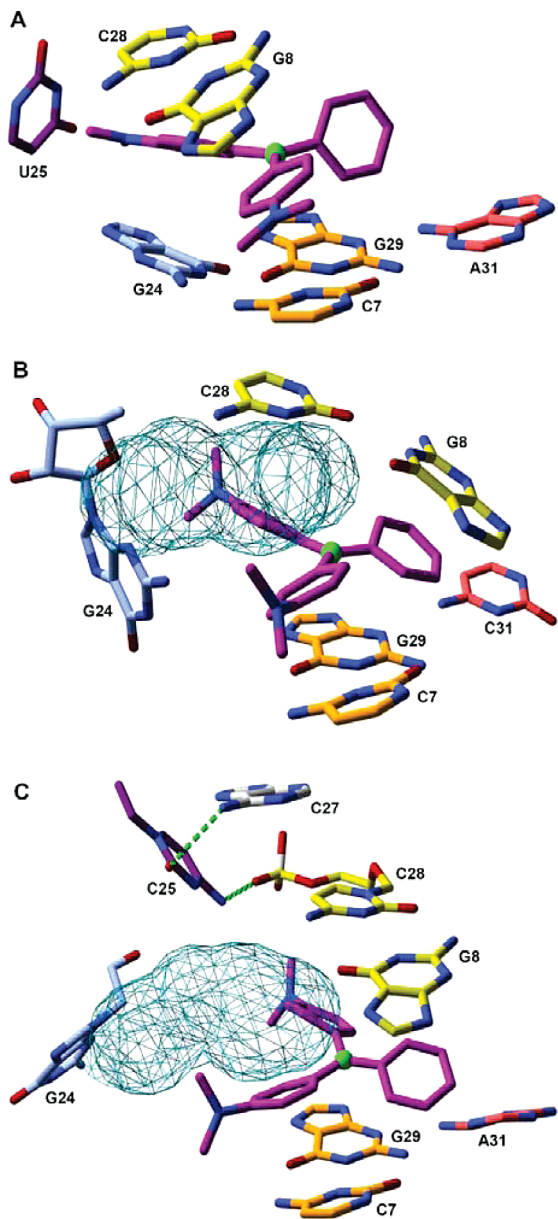


**Figure 6.** Binding pocket cavity analysis of MGA-MG variants compared with the original aptamer. (A) The binding pocket bases from the NMR structure (1Q8N.pdb, model 5) of the MGA are color-coded and demonstrate the protection that prevents hydroxide access to the C1 carbon (green) of MG (magenta). In the A31C variant (B) and U25C variant (C), rearrangement of the base quadruple (C7 and G29, orange; G24, blue; A or C31, red), the C8-G28 (yellow) base pair, and U or C25 (purple) creates a gap connecting solvent to the MG C1 carbon, which allows hydroxide access as indicated by the mesh (cyan). Note the hydrogen bonding (green dashed lines) that occurs in the U25C variant.

of MG could protect MG from  $\text{OH}^-$  attack equatorially but allow  $\text{OH}^-$  attack from the poles at the top and bottom. Cavity analysis of the MGA-MG complex showed that the MGA binding pocket further protected MG from  $\text{OH}^-$  attack from the poles. Thus, it appeared that the mechanism by which the MGA protects MG from oxidation is steric hindrance.

To evaluate the prediction made by cavity analysis, we tested the effects of several MGA variants on MG oxidation. Base replacements in the MGA binding pocket were chosen that might alter the pocket sufficiently to allow  $\text{OH}^-$  access to C1 of MG but not so much as to cause collapse of the pocket. The A31C exchange affects the base quadruple (C7-G29-G24-A31)

that sits over one side of the MG plane, and the U25C variation changes the U-turn connecting the top and bottom portions of the binding pocket. The G8C-G24C-G29C variation changes the G8-C28 and C7-G29 base pairs between which MG intercalates and was expected to completely alter the binding pocket.

The  $^1\text{H}$  NMR spectra of the MGA and its variants were consistent with their proper folding, suggesting that the pockets remained intact albeit with alterations in structure. In the absence of MG these RNAs showed 9–10 peaks in the 10–15 ppm region, which corresponds to ~9–10 base pairings in the MGA variants. These results for the MGA are consistent with its reported secondary structure.<sup>11</sup> On binding MG, the number of peaks in the 10–15 ppm region of the  $^1\text{H}$  NMR spectra increased to 13–14 in the MGA, MGA(A31C), and MGA(U25C) and decreased from 10 to 7 in the MGA(G8C-G24C-G29C). Although these results from  $^1\text{H}$  NMR spectra do not provide structural information regarding the interaction of MG inside the binding pocket of the MGA variants, they are consistent with the RNase I footprinting results and lead to the interpretation that the MG-binding pocket is formed in the MGA, MGA(A31C), and MGA(U25C) but not in the MGA(G8C-G24C-G29C) that appears to bind MG nonspecifically.

Structural changes in the binding pockets of the MGA variants are indicated by the following evidence: (1) enhanced RNase I cleavage of U32 and C31 in the MGA(A31C), (2) changed  $\lambda_{\max}$  of the MG interaction with the MGA(U25C), and (3) a significantly altered RNase I footprint of the MGA(G8C-G24C-G29C).

The  $K_d$  values of the MGA variants for MG differed widely with the MGA(G8C-G24C-G29C) showing a significant loss of affinity for MG. An intermediate change in the  $K_d$  was observed for MGA(U25C), and a negligible change in the  $K_d$  was observed for MGA(A31C). By contrast, the A31C base exchange decreases the affinity of MGA to TMR significantly.<sup>11</sup> This difference in the effect of the A31C base exchange on the affinity of MGA to MG and TMR may be due to the structural difference between MG and TMR. MG is less flat and more flexible than TMR and thus may more easily adapt to an A31C base exchange in the pocket. Although A31 makes no direct contact with MG, the A31C exchange changed a component of the base quadruple (C7-G29-G24-A31) that sits above MG in the MGA binding pocket. The U25C variation changed the base in U-turn that connects the top and bottom parts of the binding pocket.

With MG saturating each RNA (at 10–15 times its  $K_d$ ) the MGA(A31C), MGA(U25C), and MGA(G8C-G24C-G29C) were found to protect MG from oxidation in decreasing order of effectiveness with the effect of the MGA(G8C-G24C-G29C) being the same as for free MG. Whereas MGA and MGA(A31C) had similar affinities for MG but different abilities to protect MG from oxidation, MGA(A31C) and MGA(U25C) had different affinities for MG but similar abilities to protect MG from oxidation (Table 1). These results suggest that structural changes in the MGA variants compromise their abilities to protect MG from oxidation. Consistent with these observations, the combination of MD simulation followed by cavity analysis showed that the decreased effectiveness of the MGA variants to protect MG from oxidation can be explained by rearrangements in the binding pockets of the MGA variants that allow  $\text{OH}^-$  access to the C1 of MG in the pockets of MGA variants.

In addition to structural rearrangements in the binding pocket, the variant MGAs were predicted to be more mobile than the

MGA. Our MD simulations showed that the NMR-derived MGA interacted with MG with a rmsd (G8, C28, MG) of less than 0.658 Å during the simulation trajectory at equilibrium, which is not sufficiently mobile to create a gap for OH<sup>-</sup> access to the central carbon of bound MG. However, the MGA(A31C) and MGA(U25C) are more mobile than MGA. The RMSDs of (G8, C28, MG) in MGA(A31C) and MGA(U25C) reached up to 1.107 Å and 1.237 Å, respectively. Along with the structural alteration, this additional mobility promotes the existence of a gap in the G8/C28 side for OH<sup>-</sup> access to the central carbon of bound MG. It should be noted that the extent of mobility in the MD simulation of the MG-MGA aptamer depends on the structure from which the MD simulation starts. Previous MD simulations of the MGA-MG interaction showed less mobile interactions of the MG rings and MGA bases during simulation time courses that were started with the X-ray-derived MGA structure than those that were started with the NMR-derived MGA structure.<sup>40</sup>

In conclusion, in this model system, we have shown that, when sequestered in the binding pocket of its cognate aptamer, MG can be protected from attack by a molecule as small as 1.32–1.9 Å. The combined use of experimental and computational analysis provides a rational explanation of how the structural features of the aptamer binding pocket prevent hydroxyl access to the C1 of MG. Computational analysis by MD simulation and cavity analysis was also able to predict changes in the binding pockets of MGA variants that could result in the experimentally observed increase in OH<sup>-</sup> access to the C1 of MG. Thus, our results demonstrate that, although the aptamer structure is flexible and binds its target molecule by an induced fit process whereby both aptamer and target molecule change in structure, the resulting complex is sufficiently rigid to prevent the entry of as small a molecule as a hydroxyl ion.

(40) Nguyen, D. H.; Dieckmann, T.; Colvin, M. E.; Fink, W. H. *J. Phys. Chem. B* **2004**, *108*, 1279–1286.

The capability of an aptamer to wrap so snugly around its target as to prevent access of even small ions over periods of days has not been previously reported and might find application in protecting small molecules from reactive species.

The additional ability to regulate the aptamer structure with an oligonucleotide that is complementary to the aptamer binding pocket provides a means of rapidly releasing the sequestered small molecule. Aptamers can also function inside living cells. Thus, this novel finding suggests that aptamers might be used to manipulate molecular reactivity of small molecules both *in vitro* and *in vivo*.

**Acknowledgment.** Work at the Ames Laboratory was supported by the Department of Energy-Biological Systems Science Division, Office of Energy Science Research under Contract No. DE-AC02-07CH11358. We thank Mark Hargrove and Amy Andreotti for useful advice and Gaya Amarasinghe for the same and also for help in interpreting the NMR data for the MGA variants. We also thank Bruce Fulton in the Biomolecular Structure Facility and Kamel Harrata and Shu Xu in the Chemical Instrumentation Facility at Iowa State University for their technical support and advice in the NMR and mass spectrometry experiments. We thank Aimin Yan for his help on statistical analysis. We also thank the journal's anonymous reviewers for their insightful comments.

**Supporting Information Available:** pH dependence of MG oxidation; hydroxylation of MG bleaching; variations around the MGA binding pocket compromise its ability to protect MG; half lives ( $t_{1/2}$ ) of MG in the presence and absence of MGA and its variants; *P* values of Tukey multiple comparisons of half-lives ( $t_{1/2}$ ) of MG in the presence and absence of MGA and its variants; topology and parameter files for malachite green. This material is available free of charge via the Internet at <http://pubs.acs.org>.

JA902719Q